Fluid Dynamic Modeling of an Industrial Wet Chemical Process Bath for the Production of Silicon Solar Cells

L. Mohr[1], M. Zimmer[1], A. Moldovan[1], M. Menschick[2], B. Mandlmeier[2], C. Müller[3]
1. Fraunhofer Institute for Solar Energy Systems ISE, Freiburg, Germany
2. Singulus Technology AG, Fürstenfeldbruck, Germany
3. Albert-Ludwigs-Universität, Freiburg, Germany

Abstract

Simulation of the fluid flow in a present basin of a wet chemical plant gains a deeper understanding of the processes in the basin. The process solution is circulated by a pump from the supply pipe, through a perforated plate, along a carrier and over an overflow collar back to the supply pipe. For the described system a simulation procedure had to be found. The most important approximations for the simulation were: (1) The separation of the model into supply pipe and a process basin and (2) the replacement of the perforated plate by the Screen feature. It was shown that the simulation could be separated into two study steps. The relative difference of the velocity magnitude of the one and two steps simulation was 2% relatively. The fluid flow in the basin was validated by measurements with an acoustic digital flow meter. The validation was carried out, with the best consensus found in the middle of the basin with an experimental velocity of 20±4 mm/s and a simulated velocity of 19±3 mm/s. A reduction of the velocity of 87% was shown, due to the perforated plate. The Screen feature cannot be used without further adjustments on the solidity σ_S and the refractive index η.

Keywords: Computational fluid dynamic, Single-phase flow, κ-ε Turbulence model, Algebraic yPlus model, Screen feature.

1. Introduction

Silicon solar cells are produced in a series of different process steps in which wet-chemical etching and rinsing steps have a considerable influence on the quality of the wafers [1]. Etching baths are used for surface structuring or intended etch back. Examples therefore are texturing [2], cleaning and conditioning [3], or etch back of the front emitter to improve electrical properties of the solar cell [4,5]. The requirements for optimal flow conditions over each individual wafer surface are very high, since different etching rates can result from an uneven flow [6]. In order to increase the throughput in the industrial production of solar cells, wafers are processed in parallel batch processes in which two carriers with 100 wafers are dipped in a circulated process bath. Batch-type processes have been studied in several publications, the mass transfer and the kinetic effects [7], as well as the water motion [8,9]. For this study the flow in a basin should be simulated from the supply pipe to the overflow collar, by use of flow simulations. The aim was to use the obtained flow conditions for (1) a deeper understanding of the processes in the basin, (2) optimizing the basin or pipe geometry for the future and (3) to use the obtained flow conditions to investigate flow-induced etching patterns. Therefore the most important approximations, the separation of the model in the supply pipe and the process basin, as well as the replacement of the perforated plate by the Screen function were investigated. The approximations reduce computing time in later variations of geometry, or parameter, such as temperature, flow rate, number of wafers or changes in geometry.

2. Experimental Set-up

2.1. Basin structure

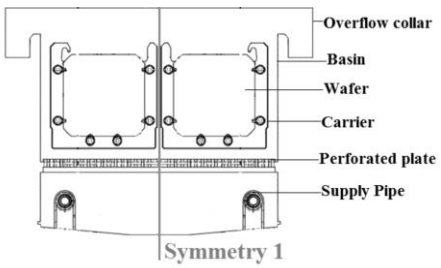

Figure 1: Scheme of the basin, with overflow collars, wafers, carriers, perforated plate, supply pipes and one of two symmetry axes.

In the basin, on which the study is focused on the process solution is circulated by a pump, which transports the solution into two supply pipes, through a perforated plate, along two carriers and over the overflow collars back to the pump (Figure 1). The basin is symmetrical; hence one of two symmetry-axes is located between the two carriers and the two supply pipes. The second symmetry-axe is located in the middle of the carrier and supply pipe (Figure 2).

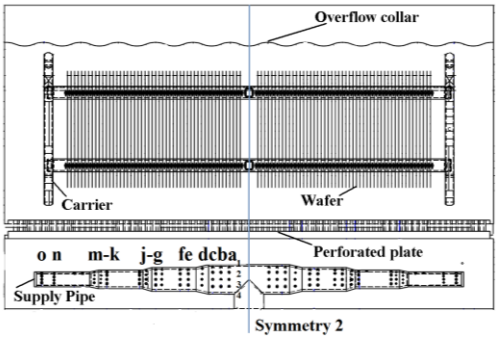

Figure 2: Side view of the basin, with overflow collar, carrier, wafer, perforated plate, supply pipe and one of two symmetry axes. The 60 outlets of the supply pipe are named from a1 till o4.

The basin contains several disturbances, with partial high scale differences, e.g. the radius of the holes in the perforated plate (3 mm) and the wafers, with a thickness of 180 µm, in the carrier show large scale differences compared to the entire basin (Figure 2). These fittings make the simulation complicate, even if only a quarter of the basin, divided by the two symmetry axes is used (Figure 1 and Figure 2). Therefore the basin was divided in smaller models: supply pipe, basin without the fittings (perforated plate, carrier, wafers) and a section of the basin with perforated plate. For all studies the Computational Fluid Dynamics (CFD) Module of COMSOL Multiphysic 5.21 was used. To keep the model simple, the simulations were carried out, using water instead of the chemical mixture as initial material. For all simulations an inlet velocity of the supply pipe of $u_0 = 0.4642$ m/s is assumed, resulting from the volume flow of the pump relative to the inlet of the supply pipe.

2.2. Supply pipe simulation

First, a three-dimensional model according to the symmetry of the supply pipe was created. The inlet is located on the bottom of the pipe, the surface next to the inlet is set to symmetry condition $u \cdot n = 0$, where u is the velocity field and n is the normal vector. When the symmetry edge is chosen, it is assumed that the wall extends indefinitely, there is no penetration condition, and the velocity is not set to zero [10] as it is the case, when the normal wall application is chosen. On the 60 outlets of the pipe, the pressure boundary condition is assumed to be $p_0 = 0$ Pa, so that the pressure depends on the reference pressure, which is defined as 101325 Pa. Since the basin is used during a process with a constant circulation rate, a stationary, rather than a transient study is used. To determine a physical model, the dimensionless Reynolds number Re of the inner tube flow with the inlet diameter d, is calculated, which gives information about the flow type (Eq. 1 and 2),

$$Re_{\text{crit}} = \frac{u_0 \cdot d}{\nu} \quad (1)$$

$$u_0 = \frac{\dot{V}}{A} = \frac{\dot{V}}{d^2 \cdot \frac{\pi}{4}} \quad (2)$$

with inlet velocity u_0, kinematic viscosity ν, volume flow $\dot{V}$ and area A. The characteristic number at which the transition from the laminar to the turbulent flow takes place is referred to critical Reynolds number Re_{crit}. In the literature, $Re_{\text{crit}} = 2320$ is reported as the number, where at $Re > Re_{\text{crit}}$ a laminar flow changes to a turbulent flow [11]. With an inlet velocity of $u_0 = 0.4642$ m/s $Re = 18600$ the flow is calculated as turbulent and the κ-ε turbulence model was used for the supply pipe simulation.

2.3. Basin without fittings simulation

Our second simulation focused on the flow conditions in the basin, without the perforated plate, the carrier and the wafers. At the outlet of the basin, the pressure was assumed to be $p_0 = 0$ Pa. The previous described two symmetries are chosen, according to Figure 1 and Figure 2. In order to save computing capacity and time, instead of using a two-phase fluid (air-water), a single-phase flow is calculated and the upper wall is selected as a slip condition. It is implicitly assumed that there are no viscous effects on the sliding wall and thus no boundary layer is formed [12]. Since the height at which the perforated plate is located is of interest for later simulations, a work plane is inserted into the model for a simplified evaluation. In addition, a finer

mesh compared to the rest of the basin can be set there, whereby the variables can be resolved more precisely. Since the fluid flows from a small flow area into a large flow area (scale 1:80), a simple turbulence model, the algebraic yPlus interface at steady-state was used. In order to save computational time, the results at the outputs of the already simulated supply pipe were used as input parameters for the second study, the flow into the basin. This procedure is appropriate in the case of later changes in the geometry, for example in case of a change in the overflow collar or in the perforated plate. It was previously investigated whether this one-way coupling is suitable, since the outflow behavior in the case of untreated outlets as a free jet differs to sudden pipe extensions. Therefore the first simulation was carried out in a two steps study, where the first study step was the previous described simulation of the supply pipe. In the second step the results on the outlet of the supply pipe are used as initial value and the basin was simulated until the overflow collar. In the second simulation, the one step study, the flow from the inlet of the pipe until the overflow collar was carried out. In order to compare the two studies, the difference between the one step and two step study was calculated on the work plane.

2.4. Validation of basin without fittings

The result of the second study was validated, using an acoustic digital flow meter for highly accurate point velocity measurement (OTT ADC sensor, Figure 3).

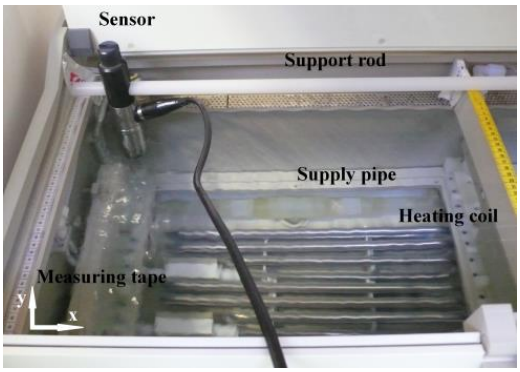

Figure 3: Top view of the basin with OTT ADC sensor, measuring tape, support rod, supply pipe and heating coil, as well as an axis orientation.

The carrier and perforated plate were removed for the experiment, only the heating rods remained in the test stand. Two measuring tapes and a support rod with markings were attached to the basin in order to position the sensor precisely. The measuring principle is based on the transmission of two short ultrasonic pulses, which are reflected on any particles in the water [13]. The phase shift of the two signals is calculated and converted into a velocity measurement. The measuring range of the OTT ADC sensor is between -0.2 m/s and 2.4 m/s. The accuracy is ± 1 % of the measured value at a resolution of 0.001 m/s. The standard measurement surface of the sensor is used to measure flow velocities in open channels, for the experiment the internal quality control setting was used. This allows the velocity to be recorded in the x-direction as well as the correlation of determination and the signal-to-noise (SNR) behavior. If no velocity of the particles is detected, neither the SNR ratio nor the correlation is correct and the value is not included in the evaluation. According to the OTT ADC specification, the measuring volume is 10 cm in front of the ultrasonic sensors, with a diameter of 1 cm per ultrasonic beam and a length of 5 cm. With a position of the sensor of 5 cm under the water surface, the exact measured point velocity in the basin 15 cm below the water surface can be measured. These results were compared with the previous simulation, therefore a plane of the velocity profile and lines according to the x and y coordinate with a thickness of 30 mm were derived from the simulation results. To get an overview of the fluid flow in the basin, 12 experimental points, three along the x-axis and four along the y-axis (Figure 3) were measured two times. Recording the velocity profile along the y-axis of the basin, three lines along the y-axis of Figure 3 were run twice within each case in 10 mm steps. The sensor was being held in position for 5 to 10 s.

2.5. Simulation of a section of the basin with perforated plate

The third simulation was focused on the effect of the perforated plate. To simplify the simulation approach, a section of the basin with a width of 81 mm was set up (Figure 4).

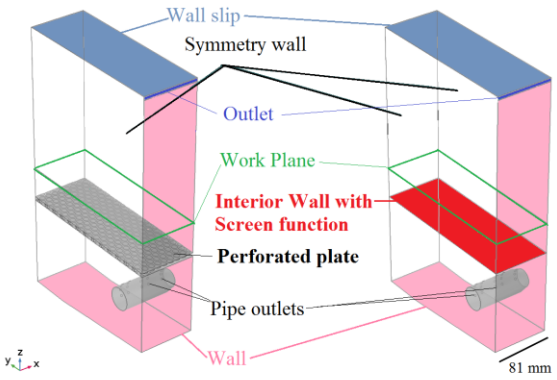

Figure 4: 81 mm section of the basin, with the perforated plate (left) and the Screen function (right).

The results of chapter 2.2 were used, to set the inlet velocity on the 20 outlets of the pipe, e1 to i4 (Figure 2). The κ-ε turbulence model was applied, since it was assumed, that turbulences below and directly above the perforated plate arise. Three out of the four side walls were set to symmetry elements. This is a strong simplification, since the inlet pipe is not symmetrical in the two x-directions. The simulation was converged by using a transient study with a step-function. The results of the perforated plate simulation (Sim_{PP}) are compared to the simulation, using the Screen feature, to investigate, whether the thickness of the plate has an effect on the flow at the location where the lower edges of the wafers are located. A work plane is added on this z-coordinate. On the interior screen wall the screen resistance K was set to "Perforated plate", the refraction coefficients η was set to $\eta = 0.8$, which was received from the simulation of the basin with perforated plate. Due to calculating the ratio between the cutting angle of the averaged vector with the entry plane of the perforated plane and the cutting angle of the averaged vector with the exit plane of the perforated plane. Two solidities σ_s (ratio of blocked to total area) are compared. Since, a hole of the plate tapers conically and diverges again in z-direction. So that $\sigma_{s1} = 0.681$ (Sim_{S1}), refers to a perforated plate with $d_1 = 6$ mm holes and $\sigma_{s2} = 0.438$ (Sim_{S1}) refers to a perforated plate with $d_2 = 5$ mm holes. This model was converged, using a transient study with a step function. The mean pressure p and velocity magnitude U, on the work plane and 10 mm under the perforated plate/interior wall (Figure 4) were compared.

3. Results and Discussion

3.1. Supply pipe

Since it can be considered that a homogeneous outflow from the supply pipe can ensure a homogeneous flow in the basin, the volume flow $\dot{V}$ out of the supply pipe was obtained by simulation. Therefore $\dot{V}$ was plotted, labeled with the number of the outlet from Figure 2, in relation to the position at the supply pipe (Figure 5).

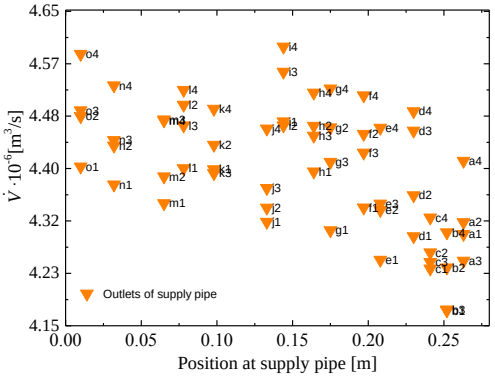

Figure 5: Volume flow $\dot{V}$ of each outlet of the supply pipe in relation to the position with numbers of the outlets.

The mean volume flow of all outlets (n = 60) is $\dot{V} = 4.4 \cdot 10^{-6} \pm 0.10 \cdot 10^{-6}$ m^3/s (mean ± standard deviation). A higher volumetric flow was generated at the lower outlets in comparison to the upper outlets of the supply pipe. The highest difference of $\dot{V} = 0.081 \cdot 10^{-6}$ m^3/s was found in row g, between g1 and g4. The lowest range was found in row c with $\dot{V} = 0.136 \cdot 10^{-6}$ m^3/s. A lower volumetric flow was produced at the first outlets (a-c) of the supply pipe (Figure 5). Due to the undisturbed inflow into the supply pipe (z-direction), turbulence was formed on the 90° deflection (Figure 6).

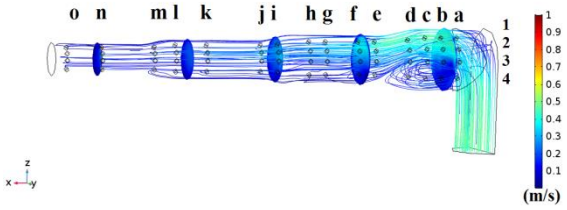

Figure 6: Velocity magnitude of the supply pipe U_{Pipe} with nomenclature of the outlets.

3.2. Basin without fittings

In order to compare the one-way coupling of the simulation procedure, the difference between the one step study and the two step study was calculated on the work plane. The mean velocity magnitude U and the mean velocity in z-direction u_z, on the work plane, from the one and the two step study reveal at 2% and 7% difference, based on the mean value of study 1 and 2 (Table 1)

Table 1: Mean velocity magnitude U and mean velocity in z-direction u_z on the work plane for study 1 and 2, as well as the differences.

Study	U (m/s)	u_z (m/s)
1. One step	$7.75 \cdot 10^{-3}$	$1.84 \cdot 10^{-3}$
2. Two step	$7.93 \cdot 10^{-3}$	$1.98 \cdot 10^{-3}$
Difference 2-1	$-0.18 \cdot 10^{-3}$	$-0.14 \cdot 10^{-3}$
Relative difference	2%	7%

The difference of 7% was acceptable to verify the two step simulation. If the flow profile on the wafer is examined, further improvements, such as grid refinement, should follow. The results of the two step study of the entire basin are shown in Figure 7.

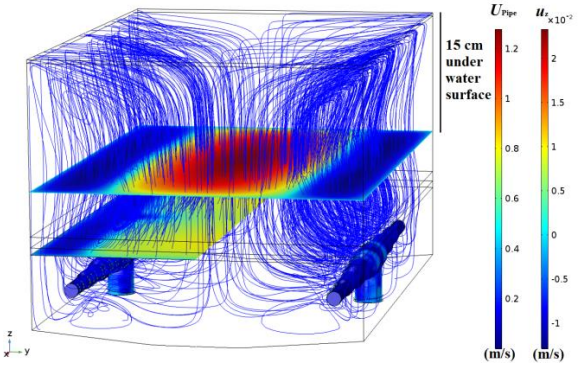

Figure 7: Two step study result of the velocity magnitude of the supply pipe U_{pipe}, the velocity in z-direction u_z at a lower and upper work plane and the streamlines.

It can be observed that turbulence develops around the supply pipe. The fluid flows from the outlets of the supply pipe, into the center of the basin, from there upwards in the direction of the overflow collars. One part of the fluid flows through the outlets of the overflow collars, the other part along the wall towards the center of the basin, so that, as can be seen on the lower work plane in turquoise, an area of less flow is formed. In particular, the blue and red areas on the upper work plane are of interest. In the center, along the x-axis, the main flow was located. At this position the two flows meet from the two supply pipes, before they flows back to the edge of the basin due to the lateral basin outlet. This is indicated by the blue region and the negative flow of the z component.

3.3. Validation of the basin without fittings

In order to identify interesting measuring points in the basin, the simulated velocities in z-direction, 15 cm below the water surface were plotted (Figure 8).

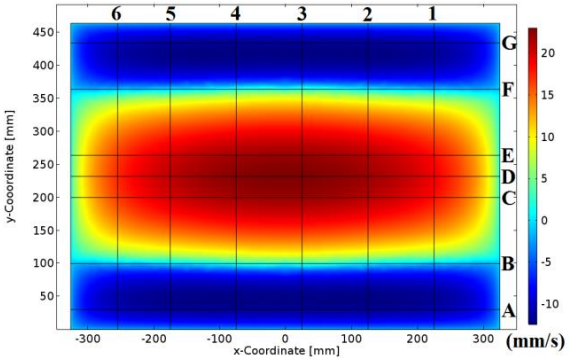

Figure 8: Velocity field in z-direction u_z, at a work plane 15 cm under the water surface and measuring points A1 to G6.

Based on this simulation, the seven regions along the y-axis (A-G) and the six regions along the x-axis (1-6) were chosen. In the validation experiment every second point (A1, C1, E1, G1, B2, etc.), the intersection of the regions, was measured with two repeats. The mean velocity in z-direction of the experimental $u_{z\,Exp}$, simulated $u_{z\,Sim}$ and the absolute value of the difference $|u_{z\,Exp} - u_{z\,Sim}|$ are shown in Table 2.

Table 2: Mean velocity in z direction of the experiment $u_{z\,Exp}$ ($n_{Exp} = 6$) and the simulation $u_{z\,Sim}$ ($n \approx 150$) for the measuring points A2 to G6 and the absolute value of difference between the experiment and the simulation $|u_{z\,Exp} - u_{z\,Sim}|$.

Line	$u_{z\,Exp}$ (mm/s)	$u_{z\,Sim}$ (mm/s)	$\lvert u_{z\,Exp} - u_{z\,Sim} \rvert$ (mm/s)
$A_{(2,4,6)}$	-16±02	-11±01	5
$B_{(1,3,5)}$	-12±03	1±05	13
$C_{(2,4,6)}$	20±04	19±03	1
$D_{(1,3,5)}$	27±09	20±03	7
$E_{(2,4,6)}$	24±05	19±03	5
$F_{(1,3,5)}$	2±13	1±05	1
$G_{(2,4,6)}$	-16±03	-11±01	5

Since only a quarter of the basin was simulated and the results were mirrored along the x and y axes, the simulation results along the x coordinate are symmetrical (Figure 9). The simulation results at A/G, B/F, and C/E are identical, due to the mirroring along the y-axis, for which reason only the four simulation series are shown (A/G, B/F, C/E, D, Figure 9).

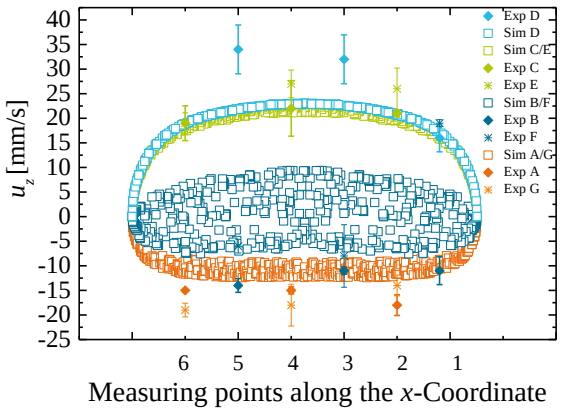

Figure 9: Experimental (closed symbols) and simulated (open symbols) velocity in z-direction u_z versus the measuring points along the x coordinate for different y coordinates (A-G).

Near the edge of the basin B/F, the simulated velocities varied little since the standard deviation along this line was high $SD_{SimB/F}$ = 5 mm/s (n = 1779), turquoise in Figure 8. This was mainly because the flow was directly opposed to the main flow (Figure 8, red area D). There was the area in which flow vortices are expected to develop (Figure 7). In the middle of the basin, a main stream was formed with 20 mm/s (Sim C/E and D); the two streams generated from the inflow pipes met and flowed towards the edge, and towards the overflow collars. A lower deviation of the velocities is in this range near to the middle of the basin, $SD_{SimC/E, D}$ = 3 mm/s, where the two streams converged and were directed upwards. Possible vortices in Sim D, due to the interference of the streams, were not considered due to the simulation setup. The results of the simulated and experimental data verified the flow directions. With the OTT flow sensor, the simulated positive and negative z-velocities shown in Figure 8 were detected and measured (Figure 9). The symmetry within the basin could be recognized in the measured z-velocities, see Exp A and Exp G. The measured velocity Exp $D_{(2,4,6)}$ = 27 ± 9 mm/s shows a higher velocity, than the simulated velocities at Sim $D_{(2,4,6)}$ = 20 ± 3 mm/s. Due to the higher velocities in the middle of the basin it was expected that the flow at the edge of the basin Exp $A_{(2,4,6)}$ = -16 ± 2 mm/ and $G_{(2,4,6)}$ = -16 ± 3 mm/s was in the higher negative range than the simulated velocities Exp $A/G_{(2,4,6,)}$ = -11 ± 1 mm/s. The open symbols in Figure 10 show the results of the simulation at line 3 depending on the y-coordinate (A-G).

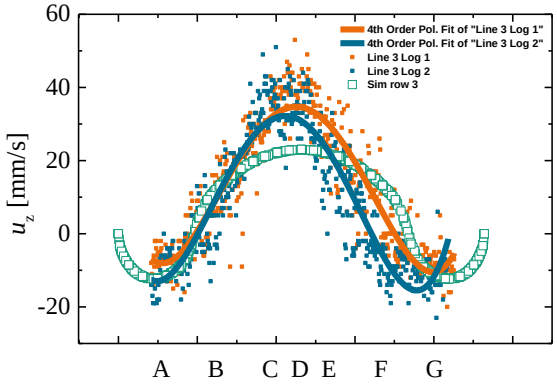

Figure 10: Experimental (closed Symbols) and simulated (open Symbols) velocity in z-direction u_z, for line 3 included the curve fittings of 4th order with R^2 = 0.86.

The experimental results measured twice of line 3 are compared with the simulation. For the experimental data, the 4th order polynomial fit was conducted. The initial and final point of the simulation could not be validated because the sensor head did not allow a measurement in direct proximity to the wall due to the geometry. The flow profile along the y-coordinate was confirmed by the experiment. The negative velocities could be validated and the maxima of the curve fittings of the measured velocities were close to the maximum of the simulated velocities: $Max_{Fit\ Log1}$ = 35 mm/s, $Max_{Fit\ Log2}$ = 32 mm/s and Max_{Sim} = 31 mm/s.

3.4. Section of the basin with fittings

The simulation of the perforated plate was performed for a time of 350 s, since it is assumed that the bath is circulated at least once in this period. The studies Sim_{S1} and Sim_{S2} with the Screen feature replacing the perforated plate could not be finalized within the set time frame,

possibly due to the set variables σ_S and η. Therefore, the results were compared at a shorter, converged time step, at 25 s (Table 3). Due to the perforated plate the velocity magnitude U decreased for 87% from below to above the perforated plate for Sim_{PP}. The simulation with the Screen feature (Sim_{S1}, Sim_{S2}) calculated approximately 33% of the velocity magnitude U_{below} with the perforated plate. Under the perforated plate the pressure is compared to the above approximately 1 Pa higher for Sim_{PP}. Almost no difference is observed for the simulation with the Screen feature. Due to these results a further adjustment on the solidity σ_S and refraction coefficient η is needed, to replace the perforated plate by the Screen feature.

Table 3: Velocity magnitude U and pressure p on a work plane 10 mm below and above the perforated plate/interior wall for the simulation with a perforated plate (Sim_{PP}), and interior wall with Screen feature with two different solidities ($Sim_{S1,2}$), at the time of 25 s.

Simulation	U_{below} (mm/s)	U_{above} (mm/s)	p_{below} (Pa)	p_{above} (Pa)
Sim_{PP}	37.1	4.8	45.93	45.06
Sim_{S1}	12.1	8.1	16.98	16.99
Sim_{S2}	12.5	8.7	16.97	16.96

4. Conclusion

The most important approximations of the procedure to simulate an actual basin were studied. The separation of the model could be done in a two steps study with a relative difference of 2% compared to a one step study. The fluid flow in the basin was validated, with the best consensus found in the middle of the basin with an experimental velocity of 20 ± 4 mm/s and a simulated velocity of 19 ± 3 mm/s. First simulations to replace the perforated plate by the Screen feature showed that the Screen feature cannot be used without further adjustments on the solidity σ_S and the refractive index η.

5. Acknowledgements

This work was funded by the German Federal Ministry for Economic Affairs and Energy „CHEOPS“ (0324056B).

References

[1] N. Johan, M. Mohamad Shahimin, S. Shaari, Texturisation of single crystalline silicon solar cell, IEEE Student Conference on Research and Development (SCOReD) (2010).

[2] H. Schröder, Micropyramidal hillocks on koh etched {100} silicon surfaces: formation, prevention and removal, Journal of Micromechanics and Microengineering (Volume 9, Number 2) (1999).

[3] E. Vazsonyi, K. de Clercq, R. Einhaus, E. van Kerschaver, K. Said, J. Poortmans, J. Szlufcik, J. Nijs, Improved anisotropic etching process for industrial texturing of silicon solar cells, Solar Energy Materials and Solar Cells 57 (2) (1999).

[4] A. Moldovan, K. Birmann, J. Rentsch, M. Zimmer, T. Gitte, J. Fittkau, Combined ozone/HF/HCl based cleaning and adjusted emitter etch-back for silicon solar cells, Diffusion and Defect Data Pt.B: Solid State Phenomena 195 (2013).

[5] A. Lachowicz, K. Ramspeck, P. Roth, M. Manole, H. Blanke, W. Hefner, E. Brouwer, B. Schum, A. Metz, Nox-Free Solution for Emitter Etch-Back. 5 pages / 27th European Photovoltaic Solar Energy Conference and Exhibition; 1846-1850 (2012).

[6] A. Moldovan, Ozonbasierte Reinigungs- und Konditionierungsverfahren für die Herstellung hocheffizienter Silizium Solarzellen, Fraunhofer Verlag, Stuttgart, 2016.

[7] M.S. Kulkarni, H.F. Erk, Acid-Based Etching of Silicon Wafers: Mass-Transfer and Kinetic Effects, J. Electrochem. Soc. 147 (1) (2000) 176.

[8] H. Habuka, S. Kobayashi, M. Kato, T. Takeuchi, M. Aihara, Water Motion in Carrierless Wet Station, J. Electrochem. Soc. 151 (12) (2004).

[9] S. Singhal, B. Elkhatib, J. Stuber, S.V. Sreenivasan, O.A. Ezekoye, Characterization of Wet Batch Cleaning Process in Advanced Semiconductor Manufacturing, IEEE Trans. Semicond. Manufact. 22 (3) (2009) 399–408.

[10] M. Günther, K. Velten, Mathematische Modellbildung und Simulation: Eine Einführung für Wissenschaftler, Ingenieure und Ökonomen, WILEY-VCH Verlag GmbH & Co. KG, Weinheim, Germany, 2014.

[11] D.W. Green, R.H. Perry, Perry's Chemical Engineers' Handbook, 8th ed., McGraw-Hill Professional Publishing, Blacklick, USA, 2007.

[12] COMSOL 5.2a (Ed.), COMSOL Multiphysics 5.2a: CFD Model User Guide, 2016.

[13] OTT Hydromet, OTT Acoustic Digital Current (ADC) Meter: User Manual, available at http://www.ott.com/en-us/products/download/ott-adc-manual-north-america/ (accessed on June 7, 2017).